Shortening the Braking Distance of a Passenger Car through Coordinated Control of Brakes and Active Suspension

Kerem Bayar[1]

ABSTRACT

Coordinated control of active suspension and brakes, is a hot research topic in academic and industrial literature. This work focuses on this area of vehicle dynamics, and proposes two methods of integrated control. Both control methods, apply the control allocation technique. In the first method which considers a vehicle equipped with a linear motor at the rear suspension, the desired control action, regarding braking, and ride comfort, is allocated to tire slips, and rear linear motor force. In the second method, a vehicle equipped with linear motors, at both front, and rear suspensions, is considered. This time the control objective is staying at the peak point of the tire force versus tire slip curve, and mitigating pitch motion as much as possible, through manipulating wheel loads. The simulation results show significant improvement in braking distance, obtained with the proposed controllers, compared to the stock vehicle, equipped with standard ABS.

Keywords: Control allocation, brake control, ABS, active suspension, braking distance

Koordine Fren - Aktif Süspansiyon Kontrolü ile Aracın Frenleme Mesafesinin Kısaltılması

ÖZ

Aktif süspansiyon – fren entegre kontrolü, akademik ve otomotiv sanayi literatüründe popüler bir araştırma konusudur. Söz konusu araştırma alanına odaklanan bu çalışma, iki entegre kontrol alternatifi önermektedir. Önerilen her iki kontrol yaklaşımı, kontrol bölüştürme yöntemini uygulamaktadır. İlk metot, aracın arka süspansiyonuna yerleştirilecek doğrusal elektrik motorları gözetilerek tasarlanmıştır. Bu metotta, aracın frenleme performansını ve sürüş konforunu geliştirecek olan kontrol sinyalleri, teker kayması, ve arka doğrusal elektrik motor kuvvetlerine bölüştürülmektedir. İkinci metot ise, hem ön, hem de arka süspansiyonlara yerleştirilecek doğrusal elektrik motorları gözetilerek tasarlanmıştır. Bu kez kontrol hedefi, teker kuvveti – teker kayması karakteristik grafiğinin pik noktasında kalmaktır. Aynı zamanda aracın yunuslama hareketi de kısıtlanmaktadır. Çalışmada özetlenen simülasyon çalışmaları ile, önerilen kontrolcülerin -pasif süspansiyonlu konvansiyonel araç ile kıyaslandığında- aracın frenleme mesafesini kısaltacağı gösterilmiştir.

Anahtar Kelimeler: Kontrol bölüştürme, fren kontrolü, ABS, aktif süspansiyon, frenleme mesafesi

1. INTRODUCTION

The number of studies focusing on active suspension control development [1], and its coordination with other control features such as vehicle stability control VSC and ABS, is increasing in academic and industrial literature. The reader is referred to [2] for a broad range of applications, along with general methods of integrated longitudinal, lateral, and vertical motion control. In [3], and [4] coordinated control of active and semi-active suspension with electronic stability control, is studied, respectively. Since this study focuses on active suspension control during straight line braking, coordinated control of active suspension and stability control is excluded from the brief literature survey given below.

In [5], control allocation method (for a fundamental comparison of different optimization methods for control allocation, the reader is referred to [6]) is applied for controlling the brakes of a vehicle equipped with semi-active suspensions. The controller is designed, such that the sprung mass acceleration, and the pitch motion of the chassis is regulated, provided the braking performance of the vehicle is not degraded.

In [7], a backstepping controller is designed, with objectives of regulating tire slip, and suppressing sprung mass acceleration. The simulation results showed the effectiveness of the developed controller, in terms of reducing the braking distance, and improving ride comfort.

In [8] it was shown through simulation results, that the braking performance of an automobile can be improved, through active suspension control. This is achieved, by controlling the brakes and active suspensions through optimization that ends up with two sprung mass motions: First one is lowering the center of gravity of the vehicle at the beginning of the braking maneuver, which reduces the load transfer. The second one is lifting the chassis to increase the loads on the wheels, towards the end of the braking maneuver. However, it is stated in this study that, optimization is inappropriate, for real time implementation, and simplified control laws are applied. Neither the optimization, nor the simplified control laws, is explicitly stated in this study.

This work focuses on shortening the braking distance of a passenger car during a hard brake maneuver on a straight line, with the help of active suspension. Two different active suspension configurations are concerned. In the first one, active suspension is only at the rear side of the vehicle. In the second one, active suspension is implemented to both front and rear sides of the vehicle. For each configuration, the applied control strategy is different. However, the two control methods have a common feature, which is the control allocation technique. This technique is applied more frequently in vehicle dynamics control literature, recently [9].

With this background, the expected contribution of this research to literature is, stating the effectiveness of the control allocation method in reducing the braking distan-

ce, through controlling active suspension and brakes, in a coordinated way, with the proposed controllers. Considering a limited number of academic publications made in the area of integrated chassis control, and the presented level of depth considering the control methods provided therein ([2] is an example), this study, stating the details of the proposed controllers explicitly, is considered to possess sufficient technical contribution to academic literature. Braking distance improvement is clearly illustrated, through simulation results. Furthermore, the second proposed control algorithm named as cordinated control in this text, treats the ABS as a black box, and manipulates the active suspension motor forces. In this sense, it is easily applicable to any production vehicle, possessing this type of active suspension system, at both front and rear sides of the vehicle.

The organization of this work is arranged as follows: In the next Section, the vehicle model used for applying the developed controllers through simulations is introduced. In Section 3, the controller development is explained in detail. In Section 4, simulation results are outlined, and in the last section, conclusions are drawn, based on the simulation results.

2. HALF CAR MODEL USED FOR CONTROL DEVELOPEMENT PURPOSE

The vehicle model used is the standard half car model, used for suspension control development purposes. It is shown in Figure 1. In the figure, k_{sf}, and k_{sr}, represent the front and rear suspension stiffness values, c_f represents the front damping coefficient, k_t is the tire stiffness and the rear damper is replaced by the linear motor, represented by F_r, capable of providing a maximum force of 2150 N at 230 V AC [10], per suspen-
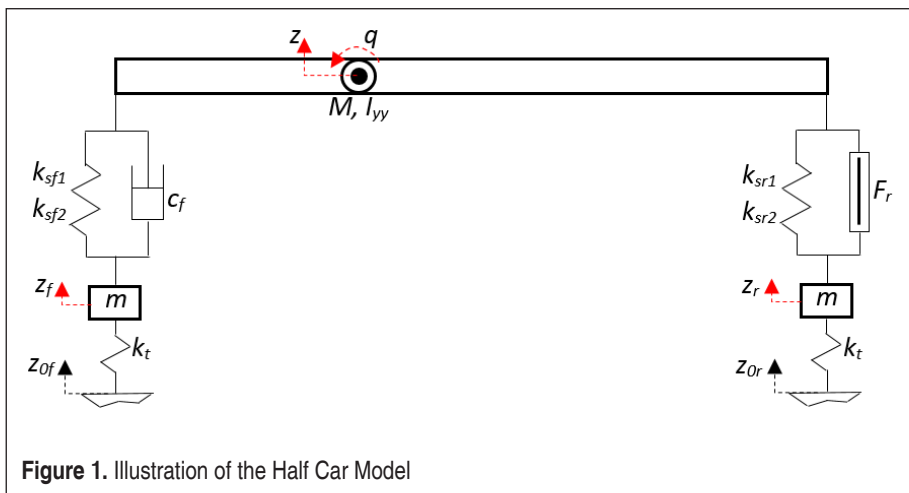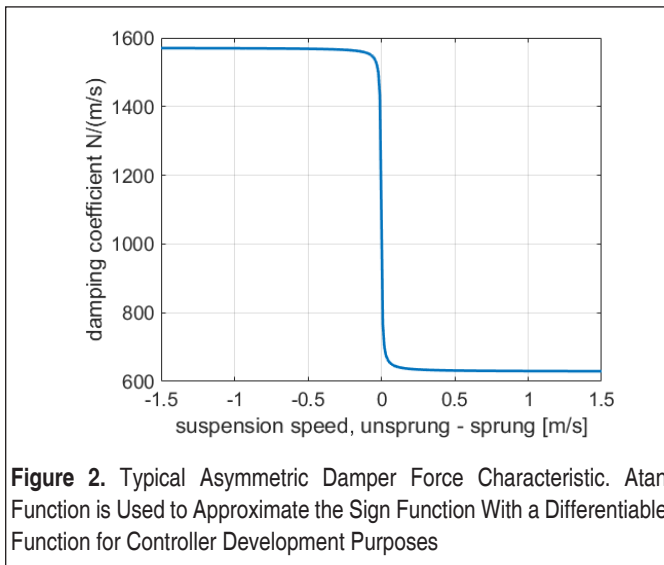

Figure 1. Illustration of the Half Car Model

sion (The F_r in Figure 1 represents the total actuator force for the rear suspensions). z_o is the road profile, z_f and z_r are the front and rear unsprung mass displacements, z is the sprung mass displacement, and q is the pitch speed. The rear damping coefficient, c_r is taken to be a low value very close to zero since there is no damper at the rear suspension; it is replaced by the linear motor.

The front damper coefficient, c_f, on the other hand, is not a constant value. It changes during jounce and rebound phases of the damper [11]. Therefore, it is modeled using an arctan function for representing this asymmetricity, using the following expression, along with the proceeding figure representing this characteristic behavior.

$$c_f = 300 \arctan(-200.susp\_speed) + 1100 \tag{1}$$

Figure 2. Typical Asymmetric Damper Force Characteristic. Atan Function is Used to Approximate the Sign Function With a Differentiable Function for Controller Development Purposes

The spring stiffness values have two components, a linear component and a non-linear component. This non-linear model is used in literature, to represent tire force more accurately [12]. This holds, especially for very high values of suspension deflection, which becomes possible considering that the damper of the suspension is replaced with the linear motor:

$$F_s = k_{s1}.z_s + k_{s2}\, z_s^3 \tag{2}$$

where z_s is the suspension deflection, k_{s1} and k_{s2} represent the linear, and the non-linear portions of the spring stiffness, and F_s represents the suspension force. With the non-linear suspension model, the equations of motion for the vertical and pitching motion

of the sprung mass, and each front and rear unsprung mass can be represented as:

$$2k_{sf1}\left(z_f + a\int q\,dt - \int V_z\,dt + d_{fo}\right) + 2k_{sf2}\left(z_f + a\int q\,dt - \int V_z\,dt + d_{fo}\right)^3$$
$$+2\left(300a\tan\left(-200\left(\dot{z}_f + aq - V_z\right)\right)+1100\right)\left(\dot{z}_f + aq - V_z\right) + 2k_{sr1}\left(z_r - b\int q\,dt - \int V_z\,dt + d_{ro}\right)$$
$$+2k_{sr2}\left(z_r - b\int q\,dt - \int V_z\,dt + d_{ro}\right)^3 + 2c_r\left(\dot{z}_r - bq - V_z\right) + F_r - M_s g = M_s\left(\dot{V}_z - V_x q\right) \tag{3}$$

$$-a\left(\begin{array}{l} 2k_{sf1}\left(z_f + a\int q\,dt - \int V_z\,dt + d_{fo}\right) + 2k_{sf2}\left(z_f + a\int q\,dt - \int V_z\,dt + d_{fo}\right)^3 \\ +2\left(300a\tan\left(-200\left(\dot{z}_f + aq - V_z\right)\right)+1100\right)\left(\dot{z}_f + aq - V_z\right) \end{array}\right)$$
$$+b\left(\begin{array}{l} 2k_{sr1}\left(z_r - b\int q\,dt - \int V_z\,dt + d_{ro}\right) \\ +2k_{sr2}\left(z_r - b\int q\,dt - \int V_z\,dt + d_{ro}\right)^3 + 2c_r\left(\dot{z}_r - bq - V_z\right) \end{array}\right) + bF_r - h\Sigma F_x = I_{yy}\dot{q} \tag{4}$$

$$k_t\left(z_{of} - z_f + d_{tof}\right) - k_{sf1}\left(z_f + a\int q\,dt - \int V_z\,dt + d_{fo}\right) - k_{sf2}\left(z_f + a\int q\,dt - \int V_z\,dt + d_{fo}\right)^3$$
$$-\left(300a\tan\left(-200\left(\dot{z}_f + aq - V_z\right)\right)+1100\right)\left(\dot{z}_f + aq - V_z\right) - mg = m\ddot{z}_f \tag{5}$$

$$k_t\left(z_{or} - z_r + d_{tor}\right) - k_{sr1}\left(z_r - b\int q\,dt - \int V_z\,dt + d_{ro}\right) - k_{sr2}\left(z_r - b\int q\,dt - \int V_z\,dt + d_{ro}\right)^3$$
$$-c_r\left(\dot{z}_r - bq - V_z\right) - mg - \frac{F_r}{2} = m\ddot{z}_r \tag{6}$$

where V_x is the longitudinal speed of the car, and d_{tof}, d_{tor}, d_{fo} and d_{ro} represent static

Table 1. Half Car Vehicle Model Parameters

	Simulator parameters
Vehicle mass [kg]	1600
Unsprung mass [kg]	46
Wheelbase [m]	2.7
Distance from cg to front axle [m]	1.2
Distance from cg to rear axle [m]	1.5
Height of center of gravity [m]	0.45
Vehicle pitch moment of inertia [kg.m²]	2000
Front suspension spring stiffness, linear portion [N/m]	15000
Front suspension spring stiffness, non-linear portion [N/m³]	6000
Rear suspension spring stiffness, linear portion [N/m]	20000
Rear suspension spring stiffness, non-linear portion [N/m³]	8000
Front suspension average damping coefficient [N.s/m]	1100
Spring stiffness of tire [N/m]	180000
Maximum linear motor force per corner [N]	2150

tire and suspension deflections. m represents the unsprung mass, and M_s represents the sprung mass. ΣF_x is the total tire longitudinal forces, and h is the distance between ground, and the pitch center height. The data set used for the half car model is provided in Table 1, below. The vehicle parameters provided in Chapter 4 of [2], and Fiat Egea [13] vehicle parameters were utilized, to make engineering guesses, about certain parameter values.

3. INTEGRATED / COORDINATED CONTROL OF BRAKES AND ACTIVE SUSPENSION

Wheel dynamics, and tire slip can be expressed as follows:

$$\dot{\omega} = \frac{T_{hs} - T_B - rF_x}{I_\omega} \tag{7}$$

$$r\omega - V = Vs + \sigma\dot{s} \tag{8}$$

where T_{hs} is the half shaft torque, T_B is the brake torque, r is tire rolling radius, F_x is tire longitudinal force, I_ω is wheel rotational inertia, ω is angular speed of the wheel, V is velocity across wheel plane, σ is the tire relaxation length, and s is tire slip. Ignoring tire relaxation length and combining these two equations yields tire slip dynamics:

$$\dot{s} = -\frac{r^2 F_x}{I_w V} - \frac{\dot{V}}{V}s - \frac{\dot{V}}{V} + \frac{r}{I_w V}T \tag{9}$$

where T is the net torque acting on the wheel. Since the tire force F_x is a function of wheel load and tire slip itself, and with the knowledge that wheel load is a function of the active suspension actuator force directly, it can be easily concluded that for a vehicle equipped with an active suspension, tire slip control would be achieved with a higher accuracy, compared to a conventional vehicle. The reason of this is the fact that the number of actuators that can contribute to tire slip regulation, increases, compared to the passive suspension vehicle, from a control standpoint. The question becomes how to distribute the control action to brake torque and linear motor. For this purpose, control allocation method is applied. The two different methods, used for this purpose, is explained in the next section.

3.1 Integrated Control of Tire Slip & Active Suspension

Figure 3 shows every section of the proposed integrated controller. The controller is composed of three main sections: 1. Generating the desired longitudinal force, vertical force and pitch moment according to the control objectives. This part is shown with the purple box in Figure 3. 2. Allocating this virtual control input onto desired
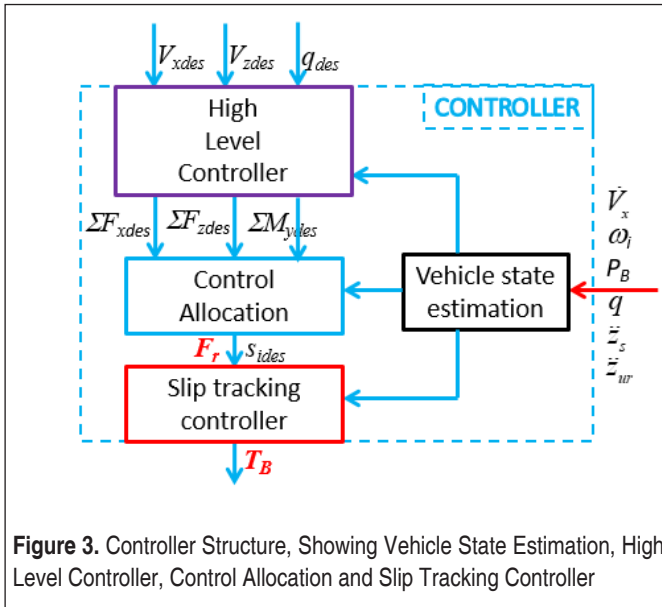
Figure 3. Controller Structure, Showing Vehicle State Estimation, High Level Controller, Control Allocation and Slip Tracking Controller

tire slip and rear motor force. This part is shown with a blue box. 3. Tracking the desired slip values with a slip tracking controller, shown with the red box. Each section of the controller is explained next, after mentioning the state estimation very briefly.

Vehicle state estimation, receives signals from the sensors, and estimates the states. Tire slip and vehicle speed estimation are carried out, using traditional method of Kalman filter [14]. Tire longitudinal forces are estimated using brake pressure information [15]. For estimating tire deflection, suspension deflection, unsprung and sprung mass speeds, pitch speed and sprung mass speed, an extended Kalman filter is developed. The equations of the Kalman filter are provided in Appendix A.

The desired vertical speed, and pitch rate, V_{zdes} and q_{des} are 0. The desired longitudinal speed, on the other hand is a ramp function going down from the initial vehicle speed at the onset of the hard brake maneuver, to 0, rapidly. This is the interpretation of the driver's brake pedal input.

For transforming the desired speeds into desired total force and moment in the high level controller, net longitudinal and vertical force, and pitch moment equations are used. The last two are already expressed by Equation 3 & Equation 4.

Equation of motion in longitudinal direction (straight line motion is considered, i.e. no yaw and roll) is given by:

$$\sum F_x - 0.047 C_D A_f V_x^2 = M \dot{V}_x \tag{10}$$

where M is total vehicle mass, C_d and A_f are the aerodynamic drag coefficient, and vehicle frontal area. $\Sigma F_x = F_{xf} + F_{xr}$, is the summation of front and rear tire longitudinal forces. Tire forces on the other hand, are expressed as a function of tire slip and normal load, with the commonly used Pacejka tire model [16].

High level controller transforms these desired speeds, to desired total force and moment, through proportional control, and some of the estimated states, by utilizing the following equations:

$$\Sigma F_{xdes} = M.K_{pVx}\left(V_{xdes} - V_x\right) + M.\dot{V}_{xdes} + 0.047 C_d A_f V_x^2$$
$$\Sigma F_{zdes} = -\Sigma \widehat{F}_s + M_s g - M_s V_x q - M_s K_{pVz} V_z \tag{11}$$
$$\Sigma M_{ydes} = -I_{yy} K_{pq} q - b\Sigma \widehat{F}_{sr} + a\Sigma \widehat{F}_{sf}$$

where M_s is sprung mass, I_{yy} is vehicle pitch inertia, a and b are distances from center of gravity to front and rear axles, respectively. $\widehat{F}_{sf}$ and $\widehat{F}_{sr}$ denote the front and rear estimated suspension forces. K_{pVx}, K_{pVz} and K_{pq} are the proportional controller gains for controlling each three speed.

Next step is allocating the virtual control input, $[\Sigma_{Fxdes}\ \Sigma_{Fzdes}\ \Sigma_{Mydes}]^{\mathrm{T}}$ onto front and rear desired slip, and the rear linear motor force. For this, the relationship between the virtual control input and control allocation variables need be derived, and this is done through the control effectiveness matrix:

$$B = \begin{bmatrix} \dfrac{\partial \Sigma F_x}{\partial s_f} & \dfrac{\partial \Sigma F_x}{\partial s_r} & \dfrac{\partial \Sigma F_x}{F_r} \\[2mm] \dfrac{\partial \Sigma F_z}{\partial s_f} & \dfrac{\partial \Sigma F_z}{\partial s_r} & \dfrac{\partial \Sigma F_z}{F_r} \\[2mm] \dfrac{\partial \Sigma M_y}{\partial s_f} & \dfrac{\partial \Sigma M_y}{\partial s_r} & \dfrac{\partial \Sigma M_y}{F_r} \end{bmatrix} \tag{12}$$

Derivation of the elements of the control effectiveness matrix is given in Appendix B.

With the derivation of the control effectiveness matrix, the control allocation problem turns into a quadratic optimization problem, with the following cost function:

$$J = \arg\min_{u} = \frac{1}{2}(Bu - v)^T W_v (Bu - v) + \frac{1}{2}u^T W_u u \tag{13}$$

where u is the vector of allocation variables, W_v and W_u are the weighting matrices for allocation accuracy, and control energy, subject to the inequality constraints:

$$u = \begin{Bmatrix} -s_f \\ -s_r \\ |F_r| \end{Bmatrix} < \begin{Bmatrix} 0.1 \\ 0.1 \\ 2150\ N \end{Bmatrix} \tag{14}$$

In other words, the brake slip values should not exceed 10%, and the motor force should be kept below its maximum limit. The allocation accuracy is specified with respect to the weighting matrix, W_v as:

$$W_v = \begin{bmatrix} w_{v1} & 0 & 0 \\ 0 & w_{v2} & 0 \\ 0 & 0 & w_{v3} \end{bmatrix} \tag{15}$$

where $w_{v1} > w_{v3} > w_{v2}$ since tracking the desired vehicle speed, is more important than ride comfort during a hard brake maneuver. Controlling pitching motion, is important though, considering its direct effect on tire longitudinal forces. That is why w_{v3}, the pitch speed weighting is picked higher than w_{v2}, sprung mass acceleration weighting. The values of the weightings, are specified with a simple trial error process.

The control energy, on the other hand, is specified with respect to the following weighting matrix:

$$W_u = \begin{bmatrix} w_s & 0 & 0 \\ 0 & w_s & 0 \\ 0 & 0 & w_{Fr} \end{bmatrix} \tag{16}$$

Fixed point algorithm [17] is used to solve this optimization problem in real time, which yields the lowest amount of floating point operations, according to [9]. The software, used to implement this algorithm, which is also used to build the simulator for this study, is Matlab – Simulink. The simple code, applied within an Embedded Matlab function, in Simulink, is provided in Appendix C.

The desired linear motor force is commanded directly to the motor. The desired tire slip values are tracked with the slip tracking sliding mode controller, explained in [18]. It is not given here again, for brevity.

It should be noted at this point, that the novelty of the proposed controller based on control allocation method, does not found on invention of a new control method. Rather, its novelty is based on applying the control allocation approach, for coordinated tire slip and active suspension control. There are not many examples of applying control allocation method, in the area of vehicle dynamics control, considering the literature survey, given in the Introduction section.

Before commenting on the simulation results comparing this control approach, with the stock ABS in the next section, another control approach is given in the next subsection.

3.2 Coordinated Control of ABS & Active Suspension

As mentioned in the previous subsection, the control method that distributes the desired longitudinal speed, vertical speed and pitch speed, onto the front and rear tire slip values, and the linear motor force at the rear suspension, requires a high level controller, and a control allocation subsystem. From a hardware standpoint, this would require a powerful supervisory controller, distributing the required control action -rear linear motor force, and brake torques- to the motor and brake control modules (ABS module). From a practical standpoint, it may not be feasible to implement such a supervisory controller, to every production vehicle.

On the other hand, if another control method is developed such that ABS is treated as a black box (meaning its software, is modifiable only at parameter level, it cannot be recoded), whereas active suspension, has the objective of keeping the normalized longitudinal force, at the peak point of the longitudinal force vs tire slip curve, then this would be more applicable to production vehicles. For instance, at a wet road surface, where the adhesion coefficient is around 0.3, the normalized longitudinal force vs tire slip curve looks like Figure 4:

Figure 4. Normalized Longitudinal Force F_x / F_z vs Tire Slip, for Wet Asphalt Road Surface.
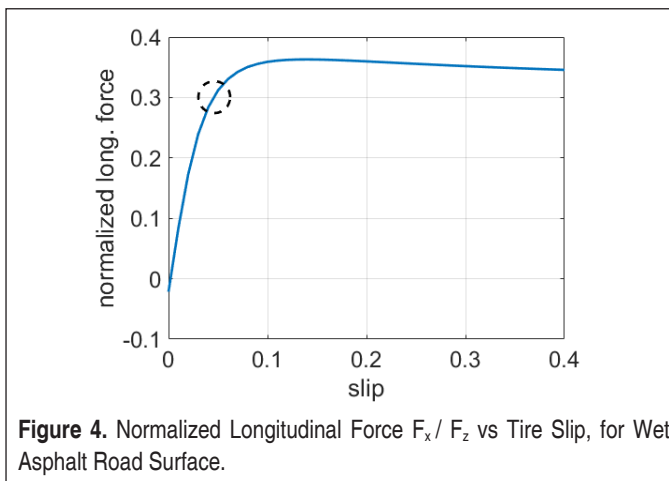
So the aforementioned simple active suspension control algorithm can be summarized as: Transmitting the estimated longitudinal force F_{x_est}, signal, from the ABS module to the active suspension control module, and setting an objective for the normal wheel load as:

$$F_{zdes} = \frac{F_{xest}}{0,3}$$

(17)

In a way, this strategy is similar to the one, of keeping the brake pulsations and normal wheel load in phase, for improving stopping distance, given in [19]:

$$F_z = Asign(T_b - \overline{T_b})$$

(18)

where F_z is the normal wheel load, T_b is the brake torque, and $\overline{T_b}$ is the mean brake torque on the wheel during braking.

The desired normal load, given by Equation 17 above, would be achieved by the linear motors, implemented to both front, and rear suspensions of the vehicle. Therefore, this time a different suspension configuration is considered. For this purpose, a simple control allocation method is used, again. Once the desired normal load is specified, the desired actuator forces can be set by the following equations:

$$F_{f\_des} = F_{zf\_des} - F_{sf\_est} - mg$$

(19)

$$F_{r\_des} = F_{zr\_des} - F_{sr\_est} - mg$$

(20)

where F_{f_des} and F_{r_des} are the desired front and rear linear motor forces, F_{sf_est} and F_{sr_est} are the estimated front and rear suspension forces. However, trying to achieve these objectives, with no control action on sprung mass acceleration, and pitch angle, does not work. Especially without controlling the pitch angle, the control idea given above fails, and this is the main reason, why control allocation method is selected to distribute the desired normal loads, pitch moment, and vertical force, to the two actuators at the front and rear suspensions.

The control allocation method can be summarized as follows:

The desired actuator forces are already given by Equations 19 & 20. The desired vertical force is given in Equation 11. The desired pitch moment, on the other hand, can be expressed with a small difference, as

$$\Sigma M_{y\_dist} = -K_{pitch}I_{yy}q - b\Sigma\widehat{F}_{sr} + a\Sigma\widehat{F}_{sf} + h\Sigma F_x$$

(21)

where ΣF_x is treated as an estimated variable now received from the ABS module, rather than a controllable variable through brake torques.

In order to allocate the virtual control input, formulated as follows:

$$v = \begin{bmatrix} F_f \\ F_r \\ \Sigma F_{z\_dist} \\ \Sigma M_{y\_dist} \end{bmatrix}$$

(22)

and defining the actuator force vector, onto which the virtual control input will be allocated:

$$u = \begin{bmatrix} F_f \\ F_r \end{bmatrix} \tag{23}$$

control effectiveness matrix can be derived as:

$$B = \frac{\partial v}{\partial u} = \begin{Bmatrix} \dfrac{\partial F_{f\_des}}{\partial u} \\ \dfrac{\partial F_{r\_des}}{\partial u} \\ \dfrac{\Sigma F_{z\_dist}}{\partial u} \\ \dfrac{\Sigma M_{y\_dist}}{\partial u} \end{Bmatrix} = \begin{bmatrix} 1 & 0 \\ 0 & 1 \\ 1 & 1 \\ -a & b \end{bmatrix} \tag{24}$$

The optimization problem, can now be stated with the following cost function

$$J = \arg\min_{U} = \frac{1}{2}(Bu - v)^T W_v (Bu - v) + \frac{1}{2}u^T W_u u \tag{25}$$

subject to

$$|u| \leq 2150 N \tag{26}$$

The control allocation problem can be stated as: Given the virtual control input v find the actuator force vector u that minimizes the cost function given by Equation 25, satisfying the constraint given by Equation 26. The weighting matrices, for allocation accuracy W_v and for control energy W_u, are given as:

$$W_v = \begin{bmatrix} w_{v1} & 0 & 0 & 0 \\ 0 & w_{v1} & 0 & 0 \\ 0 & 0 & w_{v2} & 0 \\ 0 & 0 & 0 & w_{v3} \end{bmatrix} \tag{27}$$

where w_{v1} is picked much higher than w_{v2} and w_{v3}, and
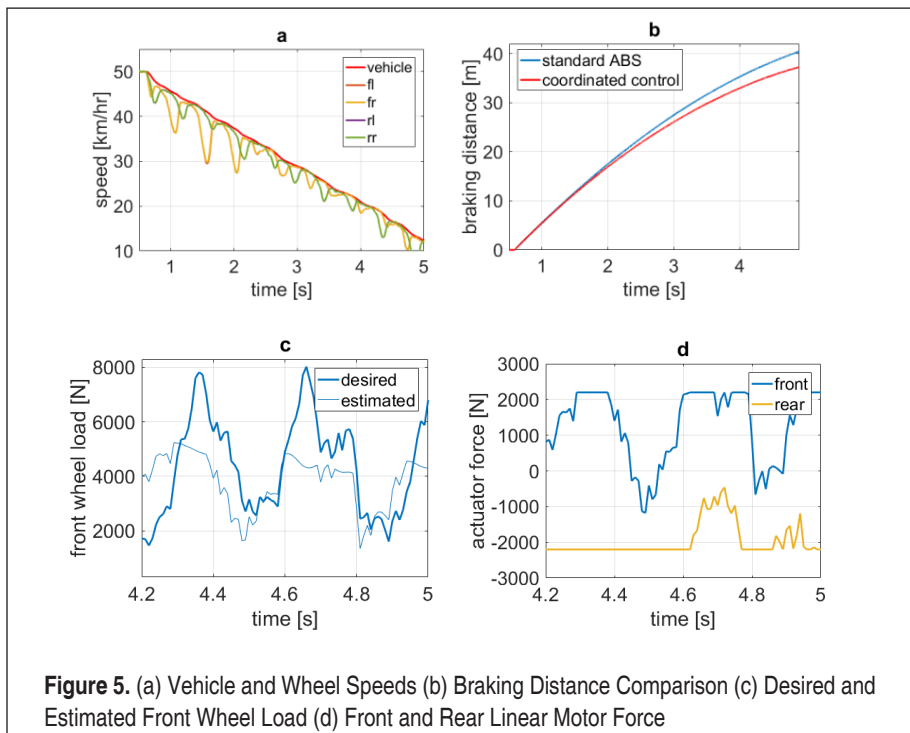
$$W_u = \begin{bmatrix} w_u & 0 \\ 0 & w_u \end{bmatrix} \tag{28}$$
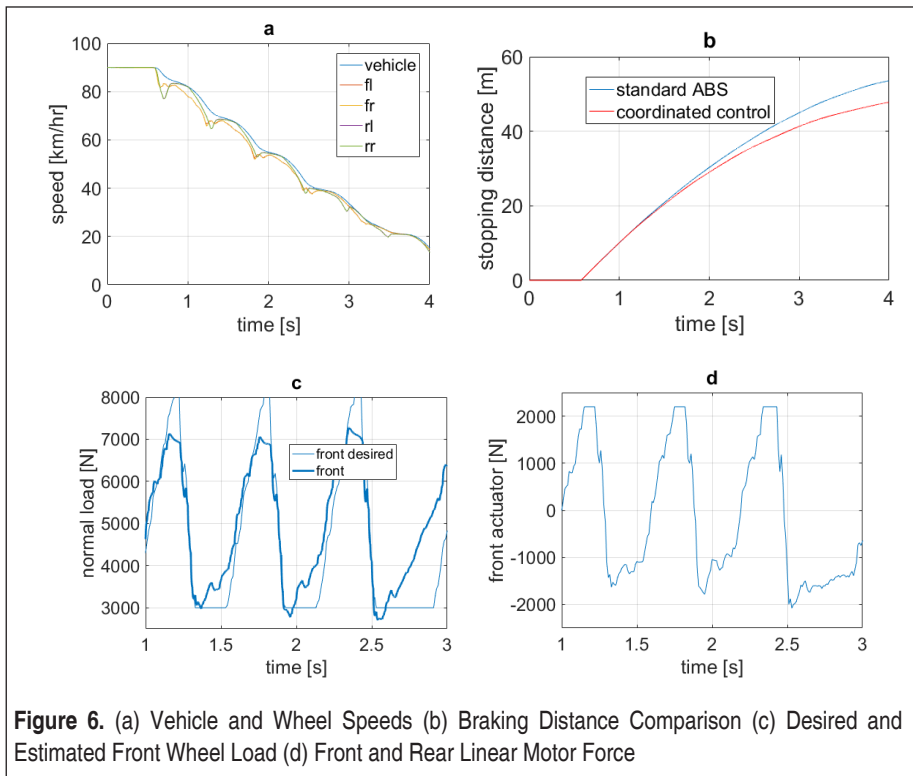
4. SIMULATION RESULTS

Figure 5 shows simulation results of applying the coordinated control strategy explained in Section 3.2, for a hard brake maneuver, where the initial vehicle speed is 50 km/hr, and the road is wet asphalt surface, with a mean adhesion coefficient of 0.3. The road profile is B-type, which has a spatial power spectral density of 0.000004 m3, with respect to [20].

The results for wheel speeds, and vehicle speed, along with the desired and estimated wheel loads, are given. Front and rear motor forces generated during the maneuver, are also given. Lastly, the 50 – 17 km/hr braking distance, is also provided (speed trends lower than that speed range, is not provided since there is no validated tire model possessing the low speed damping feature [16], that would give accurate slip trends below that speed range, used in the simulator). The braking distance result, obtained by the coordinated control strategy, is compared with the one of the standard ABS (a rule based proportional controller based on slip and wheel acceleration), applied to a vehicle, with conventional passive suspension, at both front and rear suspensions.

The comments, with respect to the results of Figure 5, can be summarized as:

Figure 5. (a) Vehicle and Wheel Speeds (b) Braking Distance Comparison (c) Desired and Estimated Front Wheel Load (d) Front and Rear Linear Motor Force

- The 50 – 17 km/hr braking distance, for the passive suspension is 40 m, whereas it is 37 m, for the active suspension vehicle. The braking distance reduction is 7.5%, a significant improvement.

- Wheel loads track the desired values good, up until around 4500 N, observed form Figure 5c. Note that perfect tracking should not be expected, because the objective of the controller, specified by the weighting factors in Equation 27, is not only tracking the desired wheel loads, but also mitigating pitch angle and sprung mass acceleration. Furthermore, the actuator forces are limited, perfect tracking is unrealizable, and actuator saturation, observed in Figure 5d, is expected.

- In the control strategy, the emphasis is given on the pitch angle, rather than sprung mass acceleration by picking $w_{v3} > w_{v2}$, because ride comfort, quantified by the sprung mass acceleration, has a minor importance during a hard brake maneuver on a relatively smoother surface like B-type road profile. Mitigating pitch angle on the other hand, is more important, considering its direct effect on braking performance.

- It can be observed from Figure 5d that the front actuators saturate at the maximum limit pushing the sprung mass up, and the rear ones doing just the opposite, pulling the

Figure 6. (a) Vehicle and Wheel Speeds (b) Braking Distance Comparison (c) Desired and Estimated Front Wheel Load (d) Front and Rear Linear Motor Force

sprung mass down. This is to avoid pitching of the sprung mass during this braking maneuver. At the same time, they help tracking the desired normal loads. For instance, towards t = 4.5 s and t=4.8 s, desired front wheel load decreases, as observed from Figure 5c, and so does the front actuator force, observed from Figure 5d.

It should be noted at this point, that there is no expectation of front and rear motor forces to be identical, during the maneuver. The controller is applying the control allocation technique, during the maneuver, explained through Equations 19-28, and adjusting the actuator forces, based on the weightings given in Equation 27 and Equation 28.

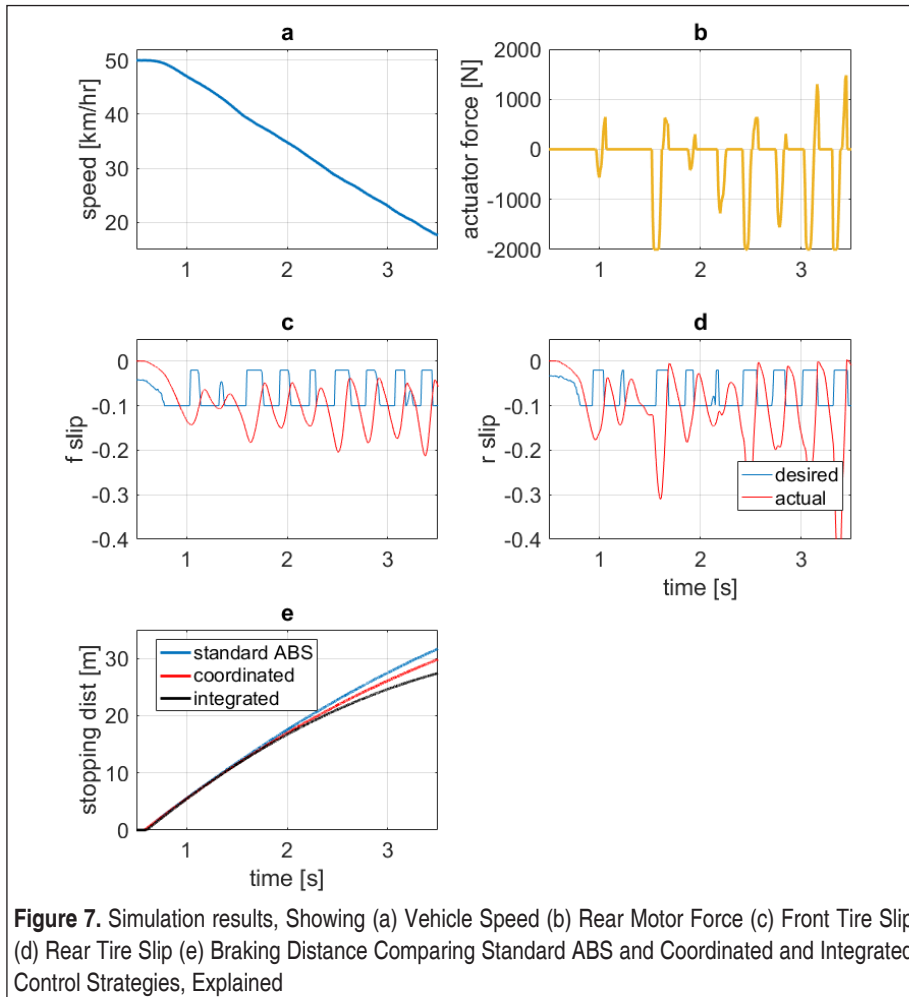The simulation results for a similar brake maneuver, this time on asphalt road profile,

Figure 7. Simulation results, Showing (a) Vehicle Speed (b) Rear Motor Force (c) Front Tire Slip (d) Rear Tire Slip (e) Braking Distance Comparing Standard ABS and Coordinated and Integrated Control Strategies, Explained

with an initial vehicle speed of 90 km/hr, are given in Figure 6. As shown in Figure 6b, 90 – 20 km/hr braking distance improvement is 11%, from 53 m with the passive suspension, to 47 m with the active one applying control allocation strategy for regulating the wheel loads, and suppressing sprung mass acceleration and pitch rate. It is also shown in Figure 6c & 6d, how the front desired wheel load is tracked, by controlling the front actuator force.

Finally, the simulation results for the first brake maneuver, on the same road profile, with the application of the integrated control strategy this time, explained in Section 3.1. is given in Figure 7. The 50 – 17 km/hr braking distance, is compared with the ones of the standard ABS, and the coordinated control strategy, in Figure 7e. The 0 – 17 km/hr braking distance is, 28 m, with the integrated control. This corresponds to a 24% improvement, compared to the stock vehicle.

Figure 7b shows how the negative rear motor force is applied frequently during maneuver. This is to avoid pitching of the sprung mass during the braking maneuver, although its priority, specified by w_{v3} in Equation 15 is lower than w_{v1}, that specifies the accuracy of tracking the desired vehicle speed.

5. CONCLUSION

Two methods of controlling active suspension and brakes in a coordinated way, is given in this work. In the first method, named as integrated control, the desired control action for braking, and minimizing vertical speed and pitching of the sprung mass, is allocated to front and rear tire slips, and the rear linear motor. In the second method, named as coordinated control, brake control module is treated as a black box, and a vehicle equipped with linear motors at both front and rear suspensions, is considered. The control objective becomes staying at the peak point of the tire force vs tire slip, through manipulating wheel loads, and controlling vertical and pitch speed of the sprung mass, simultaneously. In both cases, minimizing pitch motion of the sprung mass becomes the secondary objective, due its direct effect on brake forces, through effecting wheel loads.

Simulation results, considering B-type road profile, reveals that the 50-17 km/hr braking distance for a hard brake maneuver, on wet asphalt road surface, is reduced by 7.5% and 24%, with the coordinated and integrated control strategies, respectively, compared to the stock vehicle equipped with standard ABS. For a similar brake maneuver on the same type of road surface, this time with an initial vehicle speed of 90 km/hr, the 90-20 km/hr braking distance improvement is 11%, with the coordinated control. These results show significant improvement in shortening the braking distance, achieved by the proposed controllers.

REFERENCES

1. **Liu, H, Gao, H and Li, P.** 2014. "Handbook of Vehicle Suspension Control Systems", published by The Institution of Engineering and Technology, London, United Kingdom. ISBN: 978–1–84919–633–8.

2. **Chen, W., Xiao, H., Wang, Q., Zhao, L. and Zhu, M.** 2016. "Integrated Vehicle Dynamics and Control", published by John Wiley and Sons. ISBN: 9781118379998.

3. **Tchamna, R., Youn, E. and Youn, I.** 2014. "Combined control effects of brake and active suspension control on the global safety of a full-car non-linear model" Vehicle System Dynamics, https://doi.org/10.1080/00423114.2014.881511.

4. **Soltani, A., Bagheri, A. and Azadi, S.** 2018. "Integrated vehicle dynamics control using semi-active suspension and active braking system", Proceedings of the Institution Mechanical Engineers, Part K: Journal of Multi-body Dynamics. https://doi.org/10.1177/1464419317733186.

5. **Rupp, A.** 2013. "Control Allocation for Over-actuated Road Vehicles", MS Thesis, TU Graz, Austria.

6. **Bodson, M.** 2002. "Evaluation of Optimization Methods for Control Allocation", Journal of Guidance, Control, and Dynamics. Vol. 25, No 4. https://doi.org/10.2514/2.4937.

7. **Zhang, J., Sun, W., Liu, Z. and Zeng, M.** 2019. "Comfort braking control for brake-by-wire vehicles", Mechanical Systems and Signal Processing, https://doi.org/10.1016/j.ymssp.2019.106255.

8. **Edren, J., Jonasson, M., Jerrelind, J., Trigell, A. S. and Drugge, L.** 2015. "Utilisation of optimization solutions to control active suspension for decreased braking distance" Vehicle System Dynamics, https://doi.org/10.1080/00423114.2014.99244.

9. **Wang, J.** 2007. "Coordinated and Reconfigurable Vehicle Dynamics Control", PhD Dissertation, The University of Texas at Austin.

10. Linmot, Model P10-70x400U/150-BL-QJ Company url: https://linmot.com

11. **Dixon, J. C.** 2007 "The Shock Absorber Handbook", 2nd Edition, John Wiley & Sons, ISBN: 978-0-470-51020-9.

12. **Yang, L., Chen, W., Gao, Z. and Chen, Y.** 2014. "Nonlinear Control of Quarter Vehicle Model with Semi-active Suspension Based on Solenoid Valve Damper", Transactions of the Chinese Society of Agricultural Machinery, https://doi.org/10.6041/j.issn.1000-1298.2014.04.001.

13. Website provided at: url: www.fiat.com.tr

14. **Kiencke, U. and Nielsen, L.** 2005. "Automotive Control Systems", 2nd Edition, Springer, ISBN 3-540-23139-0.

15. **Van Zanten, A. T.** 2000. "Bosch ESP Systems: 5 Years of Experience", SAE (Society of Automotive Engineers) Paper 2000-01-1633. ISSN: 0148-7191.

16. **Pacejka, H. B.** 2012. "Tyre and Vehicle Dynamics", Elsevier/Butterworth-Heinemann. ISBN: 0080970168.

17. **Lu, P.** 1996. "Constrained tracking control of non-linear systems", Systems & Control Letters. https://doi.org/10.1016/0167-6911(95)00075-5.

18. **Bayar, K., Wang, J. and Rizzoni, G.** 2012. "Development of a vehicle stability control strategy for a hybrid electric vehicle equipped with axle motors", Proceedings of the Institution of Mechanical Engineers, Part D, Journal of Automobile Engineering. http://pid.sagepub.com/content/early/2012/01/03/0954407011433396.

19. **Alleyne, A.** 1997. "Improved Vehicle Performance Using Combined Suspension and Braking Forces", Vehicle System Dynamics, https://doi.org/10.1080/00423119708969330.

20. ISO 8608, 2016 "Mechanical Vibration – Road surface profiles – Reporting of measured data", International Standard.

APPENDİX A

The non-linear discrete state equations, taking front and rear wheel and suspension deflections, unsprung mass speeds, sprung mass and pitch speeds as the 8 states, can be written as:

$$
\begin{aligned}
x_1(k+1) &= x_1(k) - \tau x_5(k) + \tau \dot{z}_{0f}(k) \\
x_2(k+1) &= x_2(k) - \tau x_6(k) + \tau \dot{z}_{0r}(k) \\
x_3(k+1) &= x_3(k) + \tau\left(x_5(k) + ax_7(k) - x_8(k)\right) \\
x_4(k+1) &= x_4(k) + \tau\left(x_6(k) - bx_7(k) - x_8(k)\right) \\
x_5(k+1) &= x_5(k) + \tau\left(\begin{array}{c} \dfrac{k_t}{m}x_1(k) - \dfrac{k_{sf1}}{m}x_3(k) - \dfrac{k_{sf2}}{m}\left(x_3^3(k) + 3d_{f0}x_3^2(k) + 3d_{f0}^2 x_3(k)\right) \\ -\dfrac{\left[300a\tan\left(-200\left(x_5(k) + ax_7(k) - x_8(k)\right)\right) + 1100\right]\left(x_5(k) + ax_7(k) - x_8(k)\right)}{m} \end{array}\right) \\
x_6(k+1) &= x_6(k) + \tau\left(\begin{array}{c} \dfrac{k_t}{m}x_2(k) - \dfrac{k_{sr1}}{m}x_4(k) - \dfrac{k_{sr2}}{m}\left(x_4^3(k) + 3d_{r0}x_4^2(k) + 3d_{r0}^2 x_4(k)\right) \\ -\dfrac{c_r\left(x_6(k) - bx_7(k) - x_8(k)\right)}{m} \end{array}\right) - \tau\dfrac{1}{2m}F_r \\
x_7(k+1) &= x_7(k) + \tau\left(\dfrac{1}{I_{yy}}\left(2\left(\begin{array}{c} -a\left(\begin{array}{c} k_{sf1}x_3(k) + k_{sf2}\left(x_3^3(k) + 3d_{f0}x_3^2(k) + 3d_{f0}^2 x_3(k)\right) \\ +\left[300a\tan\left(-200\left(x_5(k) + ax_7(k) - x_8(k)\right)\right) + 1100\right]\left(x_5(k) + ax_7(k) - x_8(k)\right) \end{array}\right) \\ +b\left(\begin{array}{c} k_{sr1}x_4(k) + k_{sr2}\left(x_4^3(k) + 3d_{r0}x_4^2(k) + 3d_{r0}^2 x_4(k)\right) \\ +c_r\left(x_6(k) - bx_7(k) - x_8(k)\right) \end{array}\right) \end{array}\right)\right)\right) \\
&\quad + \tau\dfrac{1}{I_{yy}}bF_r - \tau\dfrac{1}{I_{yy}}h\left(\Sigma F_x\right)_{ext} \\
x_8(k+1) &= x_8(k) + \tau\left(\dfrac{1}{M_s}\left(2\left(\begin{array}{c} k_{sf1}x_3(k) + k_{sf2}\left(x_3^3(k) + 3d_{f0}x_3^2(k) + 3d_{f0}^2 x_3(k)\right) \\ +\left[300a\tan\left(-200\left(x_5(k) + ax_7(k) - x_8(k)\right)\right) + 1100\right]\left(x_5(k) + ax_7(k) - x_8(k)\right) \\ +k_{sr1}x_4(k) + k_{sr2}\left(x_4^3(k) + 3d_{r0}x_4^2(k) + 3d_{r0}^2 x_4(k)\right) + c_r\left(x_6(k) - bx_7(k) - x_8(k)\right) \end{array}\right)\right)\right) + \tau\dfrac{1}{M_s}F_r
\end{aligned}
\tag{A1}
$$

with the three measurements pitch speed, unsprung and sprung mass accelerations, the output equations:

$$
h(k) = \left[\begin{array}{c} x_7(k) \\[6pt] \dfrac{k_t}{m}x_2(k) - \dfrac{k_{sr1}}{m}x_4(k) - \dfrac{k_{sr2}}{m}\left(x_4^3(k) + 3d_{r0}x_4^2(k) + 3d_{r0}^2 x_4(k)\right) - \dfrac{c_r\left(x_6(k) - bx_7(k) - x_8(k)\right)}{m} \\[6pt] 2\left(\begin{array}{c} k_{sf1}x_3(k) + k_{sf2}\left(x_3^3(k) + 3d_{f0}x_3^2(k) + 3d_{f0}^2 x_3(k)\right) \\ +\left[300a\tan\left(-200\left(x_5(k) + ax_7(k) - x_8(k)\right)\right) + 1100\right]\left(x_5(k) + ax_7(k) - x_8(k)\right) \\ +k_{sr1}x_4(k) + k_{sr2}\left(x_4^3(k) + 3d_{r0}x_4^2(k) + 3d_{r0}^2 x_4(k)\right) + c_r\left(x_6(k) - bx_7(k) - x_8(k)\right) \end{array}\right) \end{array}\right] + \left[\begin{array}{c} 0 \\ -\dfrac{1}{2m} \\ \dfrac{1}{M_s} \end{array}\right]F_r
\tag{A2}
$$

State and state estimation covariance prediction:

$$\hat{x}_{k/k-1} = f\left(\hat{x}_{k-1/k-1}\right) + B\left(F_a\right)_{k-1} + G\left(\Sigma F_{x\_est}\right)_{k-1}$$

$$P_{k/k-1} = \phi\left(\hat{x}_{k-1/k-1}\right) P_{k-1/k-1} \phi\left(\hat{x}_{k-1/k-1}\right) + WQW^T$$

(A3)

where

$$B = \begin{bmatrix} 0 \\ 0 \\ 0 \\ 0 \\ 0 \\ -\tau\dfrac{1}{2m} \\ \tau\dfrac{1}{I_{yy}}b \\ \tau\dfrac{1}{M_s} \end{bmatrix}$$

(A4)

$$G = \begin{bmatrix} 0 \\ 0 \\ 0 \\ 0 \\ 0 \\ 0 \\ \dfrac{-\tau h}{I_{yy}} \\ 0 \end{bmatrix}$$

(A5)

$$\phi = \begin{bmatrix} \dfrac{\partial f_1}{\partial x_1} & \dfrac{\partial f_1}{\partial x_2} & \cdots & \dfrac{\partial f_1}{\partial x_7} & \dfrac{\partial f_1}{\partial x_8} \\ \dfrac{\partial f_2}{\partial x_1} & \dfrac{\partial f_2}{\partial x_2} & \cdots & \dfrac{\partial f_2}{\partial x_7} & \dfrac{\partial f_2}{\partial x_8} \\ \dfrac{\partial f_3}{\partial x_1} & \dfrac{\partial f_3}{\partial x_2} & \cdots & \dfrac{\partial f_3}{\partial x_7} & \dfrac{\partial f_3}{\partial x_8} \\ \dfrac{\partial f_4}{\partial x_1} & \dfrac{\partial f_4}{\partial x_2} & \cdots & \dfrac{\partial f_4}{\partial x_7} & \dfrac{\partial f_4}{\partial x_8} \\ \dfrac{\partial f_5}{\partial x_1} & \dfrac{\partial f_5}{\partial x_2} & \cdots & \dfrac{\partial f_5}{\partial x_7} & \dfrac{\partial f_5}{\partial x_8} \\ \dfrac{\partial f_6}{\partial x_1} & \dfrac{\partial f_6}{\partial x_2} & \cdots & \dfrac{\partial f_6}{\partial x_7} & \dfrac{\partial f_6}{\partial x_8} \\ \dfrac{\partial f_7}{\partial x_1} & \dfrac{\partial f_7}{\partial x_2} & \cdots & \dfrac{\partial f_7}{\partial x_7} & \dfrac{\partial f_7}{\partial x_8} \\ \dfrac{\partial f_8}{\partial x_1} & \dfrac{\partial f_8}{\partial x_2} & \cdots & \dfrac{\partial f_8}{\partial x_7} & \dfrac{\partial f_8}{\partial x_8} \end{bmatrix}_{@\hat{x}_{k-1/k-1}}$$

(A6)

$$W = \begin{bmatrix} \tau & 0 & 0 \\ 0 & \tau & 0 \\ 0 & 0 & 0 \\ 0 & 0 & 0 \\ 0 & 0 & 0 \\ 0 & 0 & 0 \\ 0 & 0 & \dfrac{-\tau h}{I_{yy}} \\ 0 & 0 & 0 \end{bmatrix} \qquad \text{(A7)}$$

$$Q = \begin{bmatrix} q_1 & 0 & 0 \\ 0 & q_1 & 0 \\ 0 & 0 & q_2 \end{bmatrix} \qquad \text{(A8)}$$

where q_1 is the covariance of the road profile speed, and q_2 is the covariance of the total tire force estimation error.

Kalman gain

$$K = P_{k/k-1} \left[\frac{\partial h}{\partial x}(\hat{x}_{k/k-1}) \right]^T \left\{ \left[\frac{\partial h}{\partial x}(\hat{x}_{k/k-1}) \right] P_{k/k-1} \left[\frac{\partial h}{\partial x}(\hat{x}_{k/k-1}) \right]^T + R \right\}^{-1} \qquad \text{(A9)}$$

where

$$R = \begin{bmatrix} r_1 & 0 & 0 \\ 0 & r_2 & 0 \\ 0 & 0 & r_3 \end{bmatrix} \qquad \text{(A10)}$$

with r_1 pitch speed measurement covariance, r_2, and r_3 unsprung and sprung mass accelerometer covariance values.

Finally, state and covariance update:

$$P_{k/k} = P_{k/k-1} - K \left[\frac{\partial h}{\partial x}(\hat{x}_{k/k-1}) \right] P_{k/k-1} \qquad \text{(A11)}$$

$$\hat{x}_{k/k} = \hat{x}_{k/k-1} + K \left(y - h(\hat{x}_{k/k-1}) - D(F_a)_{k-1} \right)$$

where

$$D = \begin{bmatrix} 0 \\ 0 \\ 0 \\ 0 \\ 0 \\ \dfrac{-1}{2m} \\ \dfrac{1}{I_{yy}} b \\ \dfrac{1}{M_s} \end{bmatrix} \qquad \text{(A12)}$$

Appendix B

Front and rear tire forces F_{xf} and F_{xr} are functions of tire slip and wheel load, through the Pacejka tire model. Rear wheel load, is a function of the actuator force F_r:

$$F_{zr} = F_{sr} + mg + F_r \qquad (B1)$$

where F_{sr} is the suspension force, and m is the unsprung mass. Unsprung mass acceleration is discarded from the normal load expression, to avoid unrealizable fast changes on the normal load.

Therefore, the first row of the control effectiveness matrix is obtained by deriving the variation of the total force expression with respect to front and rear tire slip, and rear actuator force, respectively. These long expressions are not given here for brevity.

Obtaining the second row is more straightforward:

$$\frac{\partial \sum F_z}{\partial s_f} = 0 \quad \frac{\partial \sum F_z}{\partial s_r} = 0 \quad \frac{\partial \sum F_z}{\partial F_r} = 1 \qquad (B2)$$

evident from Equation 1. The elements in the third row, are given as:

$$\frac{\partial \sum M_y}{\partial s_f} = -h \frac{\partial \sum F_{xf}}{\partial s_f}$$
$$\frac{\partial \sum M_y}{\partial s_r} = -h \frac{\partial \sum F_{xr}}{\partial s_r} \qquad (B3)$$

and

$$\frac{\partial \sum M_y}{F_r} \quad \text{is not given here for brevity.}$$

Appendix C

function [Uz,alphaz,nz,kz,erz,Tz] = fcn(ep_susp,W_z,W_U,Fx_dist,Fz_dist,My_dist ,x3,x4,x5,x6,x7,x8,x9,x11,Fr,dz_threshold,u_max)

v_d=transpose([Fx_dist Fz_dist My_dist]);

b11 =

b12 =

b13 =

(long expressions omitted for brevity)

b31 =

b32 =

```
b33 =
B=[b11 b12 b13;0 0 1;b31 b32 b33];
Tz=(1-ep_susp)*transpose(B)*W_z*B+ep_susp*W_U;
nz = 1/norm(Tz,'fro');
alphaz=norm(eye(3)-nz*Tz);
 kz = 1;
 U_0=transpose([0 0 0]);
 d = [0.01 0.01 1]';
 Uz = U_0;
 while norm(d)>dz_threshold
Uz=(1-ep_susp)*nz*transpose(B)*W_z*v_d-(nz*Tz-eye(3))*U_0;
d=Uz-U_0;
kz = kz + 1;
U_0=Uz;
for i=1:length(Uz)
   if ((i==1) || (i==2))
   if Uz(i)<-0.2*u_max(i) && Uz(i)>-u_max(i)
   Uz(i)=Uz(i);
   elseif Uz(i)>=-0.2*u_max(i)
      Uz(i)=-0.2*u_max(i);
   else
      Uz(i)=-u_max(i);
   end
   else
   if Uz(i)<u_max(i) && Uz(i)>-u_max(i)
      Uz(i)=Uz(i);
   elseif Uz(i)>u_max(i)
      Uz(i)=u_max(i);
   else
      Uz(i)=-u_max(i);
   end
   end
end
end
erz=norm(d);
```